Short range proximity effect induced by exchange interaction in tunnel-coupled CdTe and (Cd,Mn)Te quantum wells

E. Kirstein,[1] N. V. Kozyrev,[2] M. M. Afanasiev,[2] V. N. Mantsevich,[3,4] I. S. Krivenko,[5] V. K. Kalevich,[2] M. Salewski,[1] S. Chusnutdinow,[6] T. Wojtowicz,[6] G. Karczewski,[6] Yu. G. Kusrayev,[2] E. A. Zhukov,[1,2] D. R. Yakovlev,[1,2] and M. Bayer[1,2]

[1]*Experimentelle Physik 2, Technische Universität Dortmund, 44221 Dortmund, Germany*
[2]*Ioffe Institute, Russian Academy of Sciences, 194021 St. Petersburg, Russia*
[3]*Chair of Semiconductors and Cryoelectronics, Physics Department, Lomonosov Moscow State University, 119991 Moscow, Russia*
[4]*Quantum Technology Center, Physics Department, Lomonosov Moscow State University, 119991 Moscow, Russia*
[5]*Department of Physics, University of Michigan, Ann Arbor, Michigan 48109, USA*
[6]*Institute of Physics, Polish Academy of Sciences, 02-668 Warsaw, Poland*

(Received 25 October 2019; revised manuscript received 9 December 2019; published 9 January 2020)

The coherent spin dynamics of electrons in tunnel-coupled CdTe and (Cd,Mn)Te quantum wells (QWs) is studied by time-resolved pump-probe Kerr rotation. The coupled QWs have different thicknesses; the narrow one is doped by Mn^{2+} magnetic ions. A short range proximity effect between them is observed: the Zeeman splitting of electrons in the wide QW is given in addition to the intrinsic electron g factor by the exchange interaction with the Mn^{2+} ions mediated by electron tunneling into the narrow QW. The exchange interaction strength scales with the $Cd_{0.88}Mg_{0.12}Te$ barrier thickness separating the QWs. The Kerr rotation signal measured on the wide QW shows two close frequencies of electron spin Larmor precession in a transverse magnetic field. These components have very different spin dephasing times, 50 ps and 1 ns. The two frequencies originate from electrons in the wide QW being either part of an exciton or being resident. The proximity effect of the exciton electron is smaller due to the binding by Coulomb interaction, which decreases the tunneling to the narrow well. The experimental data are in good agreement with model calculations.

DOI: 10.1103/PhysRevB.101.035301

I. INTRODUCTION

The possibility of long-term storage of temporal coherence and ultrafast spin control in semiconductor structures defines one of the most important areas of modern spintronics [1]. An important related issue is the search of objects suitable for implementation of these features. There are various ways of solving these problems. First, one could embed magnetic ions such as Mn, Co, Fe, etc., into the semiconductor structure. In this case, the spin dynamics of the carriers and magnetic ions is determined by the strong s/p-d exchange interaction [2]. This exchange interaction between spins of free carriers and magnetic ions in diluted magnetic semiconductors (DMSs) and their heterostructures has been intensively studied [2,3]. The related surge of interest is due to the observed spin polarization effects that could potentially serve as a basis for spin generation and orientation techniques in spintronics. One of the important parameters in DMS structures is the concentration of the magnetic ions. For high and low concentrations, the mechanisms of spin relaxation can be different [4,5]. Diluted magnetic semiconductors based on II-VI materials, like (Cd,Mn)Te and (Zn,Mn)Se, have often been used as model systems to study spin-related phenomena. They demonstrate giant magneto-optical effects, e.g., the giant Zeeman splitting caused by the s/p-d exchange [6–10]. Materials of that kind can be used as spin injectors in modern nanoelectronic devices [11–14]. In that way, incorporation of magnetic ions in semiconductor heterostructures facilitates control of the electron spin polarization. The interaction with magnetic ions can also stabilize the spin orientation of localized carriers by forming magnetic polarons [15,16].

Second, control of the spin dynamics of carriers (control of their magnetization) can be efficiently provided in hybrid structures [14,17–19]. There are various types of such structures composed of different materials, for example, two semiconductor layers separated by a ferromagnetic layer; a ferromagnetic layer and a semiconductor quantum well (QW), separated by a nanometer-thick barrier; two coupled QWs of different widths separated by a thin barrier, where one QW contains magnetic ions. Hybrid structures could allow one not only to combine the functionalities of the individual constituents but also to perform mutual control of their properties. An overview of the hybrid structures and their capabilities can be found in Ref. [19]. Such structures are typically used as direct spin injection devices, where spin-polarized carriers are injected from a ferromagnet into a semiconductor [20]. One can consider the generation of spin-polarized carriers as a result of spatial separation of carriers with opposite spins caused by the influence of the magnetic ions.

In this paper we propose and implement another possibility of wave function engineering based on the modification of the overlap of electron and manganese wave functions. Namely, by changing the thickness of the multiple-monolayer-thick spacer between tunnel-coupled QWs [a wide CdTe well and a

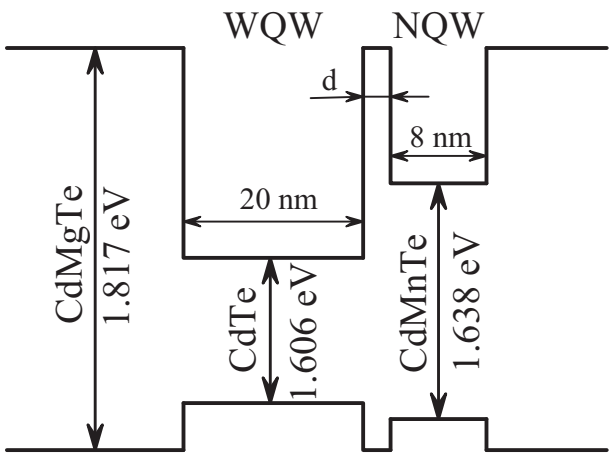

FIG. 1. Schematic energy diagram of the studied structures containing two tunnel-coupled CdTe and (Cd,Mn)Te quantum wells separated by a (Cd,Mg)Te spacer with thickness d.

narrow (Cd,Mn)Te well], the penetration depth of the electron wave function confined in the wide QW into the narrow QW is tuned. This modifies the exchange interaction strength of the electrons with the manganese ions in the narrow QW (short range proximity effect). As a result, a pronounced dependence of the electron Zeeman splitting (treated in terms of an effective electron g factor) on the spacer thickness and the sample temperature is observed. Time-resolved pump-probe Kerr rotation is used to measure the time evolution of the optically excited electron spin coherence for different experimental conditions. A theoretical model that describes the experimentally observed effects is developed.

II. EXPERIMENTAL DETAILS

The studied QW structures were grown on (100)-oriented GaAs substrates by molecular-beam epitaxy overgrown by a 4-μm $Cd_{0.88}Mg_{0.12}Te$ buffer layer to reduce the strain induced by II-VI on III-V heteroepitaxy. The heterostructures consist of two quantum wells of CdTe and $Cd_{0.984}Mn_{0.016}Te$ of 20- and 8-nm width, respectively, separated from each other by a thin $Cd_{0.88}Mg_{0.12}Te$ spacer of thickness d (Fig. 1). Only the spacer thickness differs in the samples: (1) 5 monolayers (ML; ≈1.64 nm), (2) 7 ML (≈2.30 nm), (3) 9 ML (≈2.95 nm), and (4) 11 ML (≈3.50 nm). The narrow quantum well (NQW), and thus the entire structure, was capped by a $Cd_{0.88}Mg_{0.12}Te$ layer of 50-nm width. The wide quantum well (WQW), 20 nm thick, was not intentionally doped but, nevertheless, showed some background doping. The NQW was exclusively doped with manganese.

For optical experiments the samples are placed in a cryostat offering the possibility to vary the sample temperature from 1.6 up to 300 K and to apply magnetic fields up to 6 T. The light wave vector was parallel to the sample growth axis. In the Voigt (Faraday) geometry the magnetic field B_V (B_F) is applied perpendicular (parallel) to the growth axis.

The time-resolved, degenerate pump-probe Kerr rotation (TRKR) technique [3,21] is used to study the coherent carrier spin dynamics. The pulsed emission from a mode-locked Ti:sapphire laser (pulse duration of 1.5 ps with a repetition period $T_R = 13.2$ ns) is split into the pump and probe beams. The polarization of the pump is modulated at 50 kHz between left (σ^+) and right (σ^-) circular helicity by a photoelastic modulator. The pump-induced spin coherence is detected in reflection geometry through the Kerr rotation (KR) of the linearly polarized probe beam. The spot diameter of the pump beam on the sample was 350 μm; that of the probe beam was slightly smaller. The probe power is 0.5 mW; the pump power is varied in the range 1.5–20 mW. The photon energies of the pump and probe are degenerate and tuned to be in resonance with the exciton states in the NQW and WQW in the spectral range of $\hbar\omega_{ex} = 1.55$–1.70 eV. The KR signals are measured in Voigt geometry B_V up to 3 T at different temperatures. Note that the technique used does not allow us to determine the sign of the g factor, but it is well known that the electron g factor is negative in bulk CdTe and CdTe/(Cd,Mg)Te QWs [22].

The photoluminescence (PL) spectra are excited by a continuous-wave laser with a photon energy of 2.34 eV. The reflection spectra are measured using a halogen lamp. All spectra are recorded using a 0.5-m spectrometer interfaced with a charge-coupled-device detector.

III. EXPERIMENTAL RESULTS

A. Photoluminescence and reflectivity

The PL spectra of all studied samples are shown in Fig. 2(a). At $T = 1.6$ K and $B = 0$ T each spectrum consists of two lines, which are attributed to the exciton X_{WQW} and the trion T_{WQW} recombination in the WQW [23]. Under these conditions, PL from the NQW is not observed, which suggests that charge carriers (highly likely electrons) photoexcited in the NQW rapidly tunnel into the WQW through the thin spacer. The studied samples vary only with respect to the spacer width between the QWs. Therefore, their spectra shift slightly in energy.

In order to identify the states in the NQW we measure a magnetic field series of a σ^+ and σ^- circularly polarized reflectivity spectrum in the Faraday configuration. As one can see in Figs. 2(b) and 2(c), the reflectivity spectra at $T = 1.6$ K show a narrow resonance for $B_F = 0$ T with energy of 1.602 eV and a weak shoulder at 1.66 eV, which correspond to the excitons in the WQW and NQW, respectively. With increasing magnetic field the Zeeman splitting of the excitons is observed. For the exciton in the NQW it is much larger than in the WQW. The exciton resonances are superimposed on an oscillating background originating from interference effects due to the layer sequence of the sample. The shifts of the WQW and NQW exciton energies in the magnetic field B_F are shown in Fig. 2(d) for the opposite polarizations. From the giant Zeeman splitting of the NQW excitons we evaluate the manganese concentration of $x = 0.016$. Here we neglect the rather small leakage of the wave function of the NQW exciton into the barriers and WQW, which does not exceed 5%, and use the equation for the giant Zeeman splitting in bulk $Cd_{1-x}Mn_xTe$ [2],

$$\Delta E_Z^X = g_X \mu_B B + N_0(\alpha - \beta)x\langle S_z(B,T)\rangle_{Mn}. \quad (1)$$

Here the first term on the right-hand side describes the intrinsic Zeeman splitting of the excitons without accounting

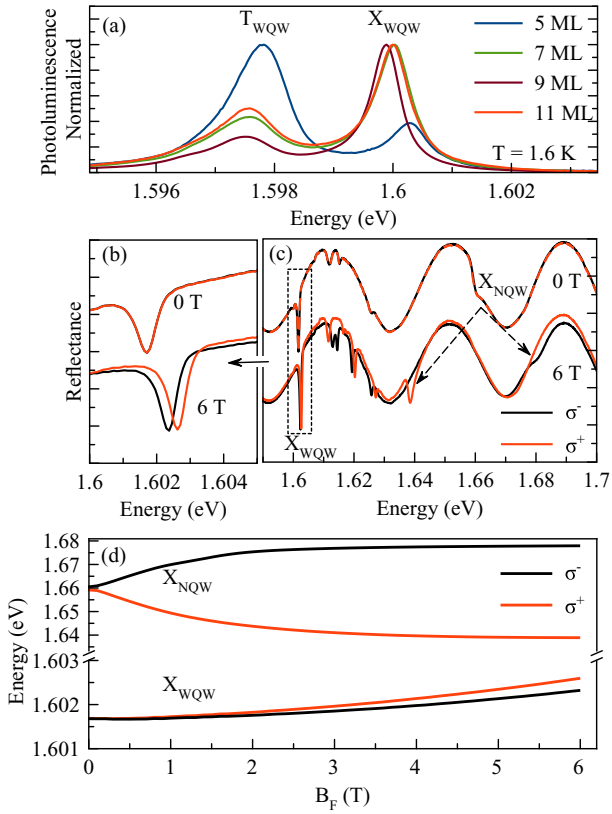

FIG. 2. (a) Photoluminescence spectra of the studied samples. $B = 0$ T. (b) Reflectivity spectra of the 11-ML sample measured for σ^-(black line) and σ^+ (red line) polarizations at $B_F = 0$ and 6 T in the spectral range of the exciton in the WQW. (c) The same spectra as in (b) in the wider spectral range covering the WQW and NQW excitons. (d) Magnetic field dependence of the exciton energy in the WQW and NQW for opposite circular polarizations. $T = 1.6$ K.

for their interaction with the Mn^{2+} ions. g_X is the exciton g factor, and μ_B is the Bohr magneton. The second term is specific for DMS. It is proportional to the average spin polarization of the Mn^{2+} ions $\langle S_z(B,T)\rangle_{\rm Mn}$. $N_0\alpha$ and $N_0\beta$ are the exchange constants for the conduction band electrons and valence band holes, respectively. In $Cd_{1-x}Mn_xTe$, $N_0\alpha = 0.22$ eV, and $N_0\beta = -0.88$ eV [24].

One can see in Fig. 2(d) that the exciton Zeeman splitting in the NQW saturates in strong fields, reaching a value of about 39 meV, which strongly exceeds the typical values of the splittings in nonmagnetic semiconductors, which are smaller than 1 meV in the applied magnetic field range. This evidences that the exchange part of the splitting dominates for the excitons in the NQW, which is also in line with the fact that the lower-in-energy exciton component is σ^+ circularly polarized.

The exciton of the WQW in the 11-ML sample has a very small overlap with the Mn^{2+} ions in the NQW. As a result, the WQW exciton Zeeman splitting is mainly controlled by the intrinsic exciton g factor g_X. It increases about linearly with magnetic field, reaching 0.27 meV at $B = 6$ T. Also, the lower-in-energy component is σ^- circularly polarized, which is characteristic for CdTe/(Cd,Mg)Te QWs [23]. It is important to note that for the WQW exciton the exchange term in the Zeeman splitting is contributed by the hole and electron wave functions penetrating into the NQW, but in a different way. Therefore, the exchange term in Eq. (1) has to be multiplied by the coefficients characterizing the penetration. In the following, we present experimental data of pump-probe Kerr rotation experiments in which the coherent spin precession of the electrons is measured. Therefore, we give here only the equation for the electron giant Zeeman splitting

$$\Delta E_Z^e = g_e\mu_B B + N_0\alpha x|\Psi_{e-Mn}|^2\langle S_z(B,T)\rangle_{\rm Mn} \equiv g_{e,\rm eff}(B,T)\mu_B B. \quad (2)$$

The first term on the right-hand side describes the intrinsic Zeeman splitting of the electrons with g factor g_e. The second exchange term is proportional to $|\Psi_{e-Mn}|^2$, which is the square of the overlap integral of the electron wave function with the Mn^{2+} ions. It is about equal to unity for the electron excited in the NQW, and it is much smaller than unity for the electron confined in the WQW. In some cases it is convenient to introduce the effective g factor $g_{e,\rm eff}(B,T)$, which accounts for both the intrinsic and exchange effects. As a consequence, $g_{e,\rm eff}$ depends on temperature (not only through the band gap but also through the average Mn polarization) and magnetic field. In the pump-probe experiments we use relatively weak magnetic fields of 0.5 or 1 T, where the field dependence of $g_{e,\rm eff}$ is very small, but the $g_{e,\rm eff}$ temperature dependence is evident. We will use it to evaluate the exchange contribution. In order to simplify the notation, we will omit below the indices e and eff for the electron g factors.

B. Time-resolved Kerr rotation

In transversal magnetic field B_V the KR signal contains several superimposed oscillating components, each of which corresponds to different Larmor precession frequencies, spin dephasing times, amplitudes, and initial phases which originate from different spin ensembles. However, the diversity

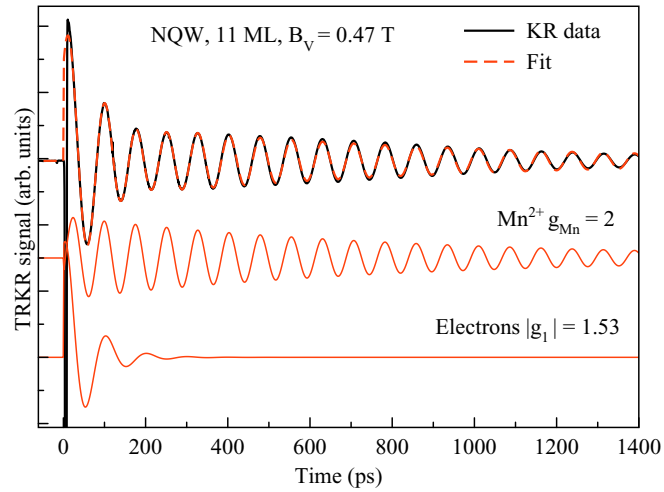

FIG. 3. Kerr rotation signals from the NQW in the 11-ML sample at $B_V = 0.47$ T. The components included in the fit are shifted vertically for clarity (solid red lines). $\hbar\omega_{\rm ex} = 1.657$ eV, $T = 5$ K, and $P_{\rm pump} = 5$ mW.

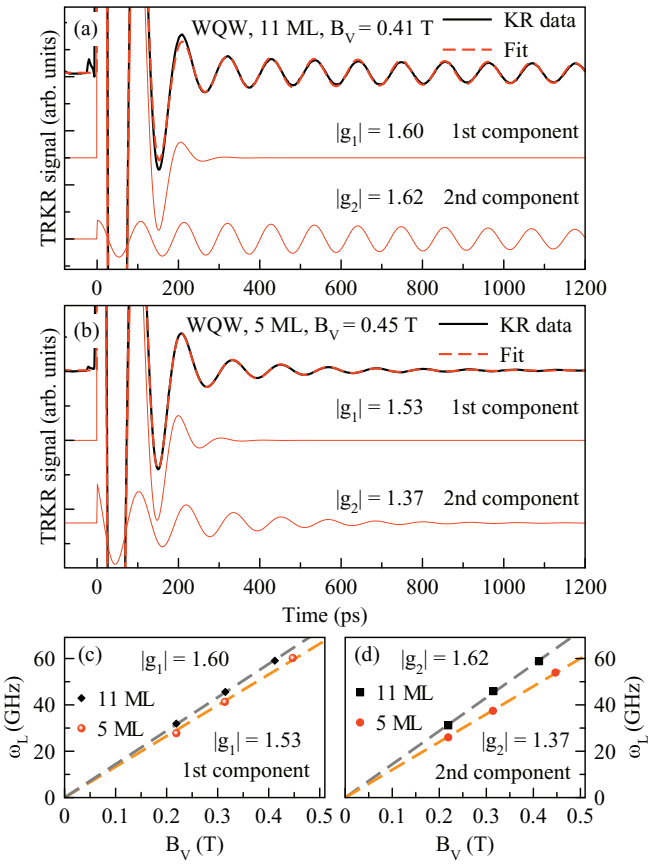

FIG. 4. Kerr rotation signals obtained from the WQW in the (a) 11-ML and (b) 5-ML samples. The components included in the fit are shifted vertically for clarity (solid red lines). Larmor frequency dependencies on magnetic field B_V for (c) the first (short T_2^*) and (d) the second (long T_2^*) oscillating components. $\hbar\omega_{ex} = 1.599$ eV, $T = 5$ K, and $P_{pump} = 5$ mW.

of signals can be divided into two groups depending on the excitation energy. The signals have significantly different KR components when excited with an energy corresponding to the NQW exciton, where electron and manganese components are observed (Fig. 3), and with an energy corresponding to the WQW exciton, where only electron components are detected (Fig. 4). We fit the Kerr rotation signals with the following equation:

$$\mathrm{KR} = \sum_i A_i \exp\left(-\frac{t}{T_{2,i}^*}\right)\sin(\omega_{L,i}t + \phi_i). \qquad (3)$$

Here the index i designates the contributing components with the following parameters: A_i is the amplitude, $T_{2,i}^*$ is the dephasing time, $\omega_{L,i} = \mu_B g_i B/\hbar$ is the Larmor precession frequency with the Landé factor g_i, $\hbar$ is the Planck constant, and ϕ_i is the phase.

Figure 3 shows a typical KR signal for the 11-ML sample excited in the NQW with $\hbar\omega_{ex} = 1.657$ eV, measured at $B_V = 0.47$ T. The signal consists of two oscillating components, whose g factors are calculated from the Larmor frequencies. One of these components corresponds to $g_{Mn} = 2$ and does not depend on temperature, spacer thickness, and magnetic field strength. Therefore, we assign the oscillations with g_{Mn}

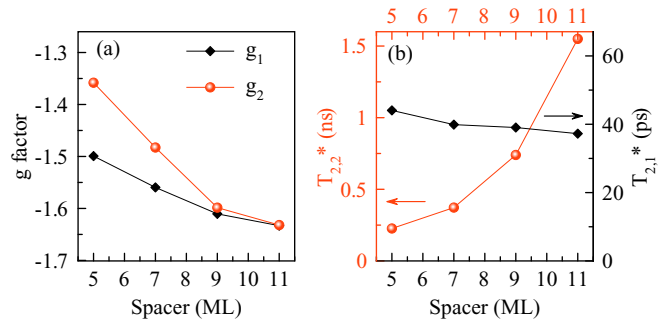

FIG. 5. Spacer thickness dependence (a) of the g factors for the first (black squares) and second (red circles) components and (b) of the spin dephasing time for both components. $T = 4.7$ K, $B = 0.4$ T. Experimental data are given by symbols, and lines are guides to the eye.

to the Larmor precession of the Mn^{2+} spins. Having in mind the large exciton Zeeman splitting in the NQW as shown in Fig. 2(d), we expect to have an electron component with large $|g| \gg 10$. However, we do not observe it, which can be explained by a very fast dephasing of this component within 10–30 ps [2,3]. Surprisingly, the KR signal has a component with a Larmor frequency corresponding to $|g_1| = 1.53$. We assign this precession to electrons confined in the WQW. Their spin beats are detected due to the exchange coupling with energetically higher lying states in the NQW. The corresponding mechanism and the consequences for the electron spin dynamics will be discussed below. Note that very similar results are obtained also for the other NQW samples with different spacer thicknesses.

The situation changes significantly for excitation in the WQW at 1.599 eV. As shown in Fig. 4(a) for the 11-ML sample and all other spacer thicknesses, the signal no longer contains the component of the manganese spin precession with $g_{Mn} = 2$. Instead, two electron components, which are very different in amplitude and spin dephasing times, are observed. Independent of spacer thickness the first component has the larger amplitude [Figs. 4(a) and 4(b)], which is more than one order of magnitude larger than that of the second component, and the shorter spin dephasing time $T_{2,1}^* \approx 35$ ps. The second component shows $T_{2,2}^* \approx 1$ ns at weak magnetic fields. In the 11-ML sample, $|g_1| = 1.60$ and $|g_2| = 1.62$ are measured. These g factor values correspond to electrons in the CdTe WQW which undergo a small renormalization due to confinement in comparison to the CdTe bulk value of -1.64 [22]. As mentioned, the electron g factor in CdTe is negative. Because the exchange contribution in the WQW is rather small, it does not overcome the intrinsic g_e, so we assign negative signs to the measured values in the following. In contrast to the 11-ML sample, in the 5-ML sample the g values measured for the WQW are different: $|g_1| = 1.53$ and $|g_2| = 1.37$ [Fig. 4(b)]. We attribute these changes to the short range proximity effect. In the case of a small spacer between the QWs, the electron wave function confined in the WQW exhibits a nonzero overlap with the Mn^{2+} spins in the NQW.

The dependencies of the g factors of both components on the spacer thickness are shown in Fig. 5(a), where clear monotonic behaviors are seen. Figure 5(b) shows the dependencies

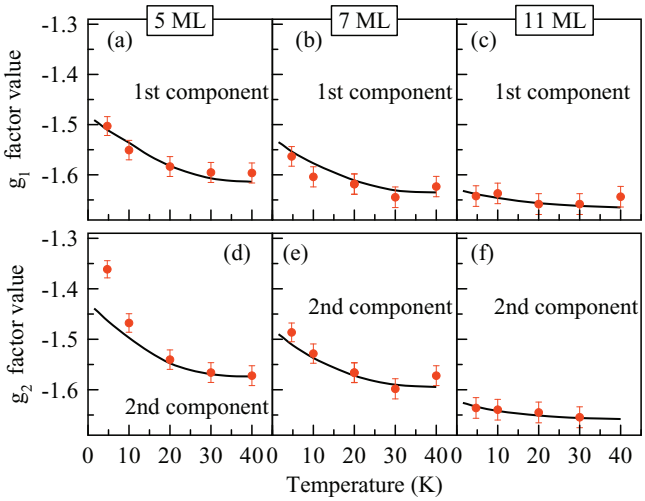

FIG. 6. Temperature dependence of the g factors for the (a)–(c) first and (d)–(f) second electron components in the samples with different spacer thicknesses. Red circles are experimental data, and black lines are the result of the theoretical calculations. B_V = 0.4 T.

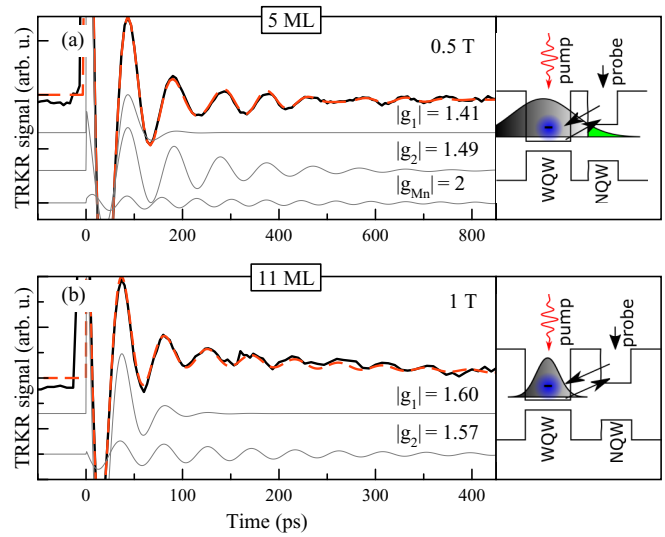

FIG. 7. Two-color pump-probe measurements of the 11-ML and 5-ML samples. The sketch in each plot shows that the WQW is pumped and the KR signal of the NQW is probed. T = 1.6 K.

of the spin dephasing times on the spacer thickness. In contrast to the first (fast) component, for the second component a strong dependence of the spin dephasing time on d is observed. With the decreasing thickness the $T^*_{2,2}$ time decreases sevenfold due to the increasing ensemble inhomogeneity from increasing the wave function overlap with Mn^{2+}.

When measuring the g factors at different temperatures for the samples with varying spacers, we find pronounced temperature dependencies (Fig. 6). This is the expected behavior because the exchange contribution to the electron Zeeman splitting is expected to decrease for increasing temperatures at which the Mn^{2+} spins become depolarized. The dependencies are qualitatively similar for the first and second components, but quantitatively, the decrease is more pronounced for the second one. For the 5-ML sample, the temperature increase from 5 to 40 K leads to a decrease in g_1 from -1.53 to -1.60 [Fig. 6(a)], while g_2 changes from -1.37 to -1.57 [Fig. 6(d)]. For samples with a larger spacer thickness the temperature dependence of both components is much weaker. In particular, it is practically absent in the 11-ML sample [Figs. 6(c) and 6(f)].

The presence of two components with different amplitudes, decay times, and frequencies in the oscillating KR signal indicates that resonant excitation of the WQW results in spin polarization of two different electron subensembles. The trion line in the PL spectrum in Fig. 2(a) indicates that the resonant photogeneration of excitons is accompanied by the formation of trions, which is possible only if there are resident charge carriers in the WQW. Since we observe oscillations with $g_{1,2} \approx -1.6$, while the heavy-hole g factor in the QW plane is negligibly small [25] (we do not observe a hole component in the KR signal), we conclude that the resident carriers are electrons. The presence of two electron components can be explained as follows: we suggest that the first (fast-decaying) component with larger amplitude is due to the spin precession of electrons bound within excitons. Its spin dephasing time is limited to the exciton lifetime, given by its recombination or binding to a trion). The second (slowly decaying) component originates from the Larmor precession of resident electrons [26], whose lifetime is not limited by recombination. Therefore, the spin dephasing time in this case is limited by the spin relaxation of resident electrons.

To clarify the origin of the g factor dependencies, additional pump-probe Kerr rotation measurements in the two-color regime are performed. We use an experimental configuration where the WQW is excited, and detection is set to the NQW. Results for the 5-ML and 11-ML samples are given in Fig. 7. Note that although the energy levels of the tunnel-coupled QW system have to be treated as joint levels, the lowest-energy state can be attributed mostly to the WQW, while the higher-energy state can be assigned dominantly to the NQW.

In the 5-ML sample [Fig. 7(a)] three oscillating components are found with parameters $g_1 = -1.41$, $T^*_{2,1} = 30$ ps; $g_2 = -1.49$, $T^*_{2,2} = 170$ ps; and $g_{Mn} = 2$, and $T^*_{2,Mn} = 340$ ps. The dynamics obtained with the two-color technique do not differ too much from that measured for resonant excitation of the NQW (see Fig. 3). Note that the coherent spin dynamics of the WQW electrons can be detected via probing exciton states in the NQW, which is possible because of the finite probability of electron wave function tunneling from the NQW into the WQW. More important, the overlap of the wave functions of the photogenerated carriers in the WQW with the Mn ions localized in the NQW is sufficient to introduce an exchange field which triggers the precession of the Mn^{2+} spins.

In contrast, in the 11-ML sample [Fig. 7(b)] the oscillation of the Mn^{2+} spins is absent. Only two Larmor components are found with the following parameters: $g_1 = -1.60$, $T^*_{2,1} = 22$ ps and $g_2 = -1.57$, $T^*_{2,2} = 160$ ps. By increasing the spacer thickness by a factor of about 2 the tipping exchange field leading to the Mn^{2+} spin precession vanishes, so that only spin precession of electrons similar to the case in Fig. 4 shows up.

As can be seen from the dependencies shown in this section, the parameters of the electrons in the WQW strongly depend on the spacer thickness. For a thin spacer, the electron wave function more strongly penetrates from the WQW into the NQW, leading to a stronger interaction with manganese. In particular, this leads to a decrease of the spin relaxation time of the second precession component in the sample with a 5-ML spacer [Fig. 5(b)] and the appearance of a manganese component in the KR signal in the two-color measurement [Fig. 7(a)]. We emphasize that the exchange interaction of the electrons bound in excitons with the manganese ions is expected to be weaker than for the resident electrons. This is the result of the additional localization caused by the Coulomb interaction within the exciton; more details are given in Sec. IV.

IV. THEORETICAL MODEL

To reveal the role of the Mn doping of one of the QWs, we describe the heterostructure by means of the envelope function model [27] for the electrons. Within the envelope function approach, the effective single-electron Hamiltonian is written in terms of a position-dependent, piecewise-constant effective mass $m^*(z)$ and an external potential $V(z)$. In each of the heterostructure layers, the effective mass is given by the bulk effective mass of the corresponding material, while its band gap defines $V(z)$. We include holes in the model to describe the ground exciton state by considering an additional electron confinement due to the adiabatic Coulomb potential created by the hole in the exciton. To analyze the results for resident electrons we neglect any contributions caused by the holes and consider the exchange interaction between a resident electron and manganese ions to be stronger than the corresponding interaction for an electron bound in an exciton state. Following the results obtained in Ref. [28], the electron-hole Coulomb interaction decreases the penetration of the electron wave function into the barriers by about 20%. The wave function of a resident electron is more extended compared to an electron in an exciton. Therefore, the exchange interaction between a resident electron and the manganese ions is stronger than for electrons in an exciton. In our calculations we consider an exchange interaction increase for a resident electron by 15%.

The Hamiltonian of the model consists of two terms,

$$\hat{H} = \hat{H}_e + \hat{H}_{\rm ex}. \tag{4}$$

The first term $\hat{H}_e$ describes a Γ_6 conduction band electron in the heterostructure, whose energy levels are Zeeman split in the external magnetic field B,

$$\hat{H}_e = \frac{\mathbf{p}^2}{2m_e(z)} + E_g + V(z) + g_e\mu_B\frac{\hat{\sigma}_z}{2}B. \tag{5}$$

Here, μ_B is the Bohr magneton, and $\hat{\sigma}_z$ is the Pauli matrix acting in the electron spin space. The potential $V(z)$ is derived from the z-dependent band gap, $V(z) = [E(z) - E_g]/2$ (the gaps of all constituent materials are centered around the same level). The zero-energy point is chosen to be at the top of the valence band of CdTe, and $E_g = 1.606$ eV denotes its band gap.

Assuming the interfaces are mathematically abrupt, one can write $E(z)$ as a piecewise-constant function with the corresponding values of $E(z)$ for $Cd_{0.88}Mg_{0.12}Te$ (1.817 eV) [29], CdTe (1.606 eV) and $Cd_{0.984}Mn_{0.016}Te$ (1.638 eV) [30]. In the NQW, some of the cadmium atoms are substituted with Mn^{2+} ions, each of which carries a localized magnetic moment $S_{\rm Mn} = 5/2$ arising from the d^5 electrons. The Zeeman splitting of the Γ_6 conduction band in magnetic field caused by the exchange interaction with the manganese ions can be described on the mean-field level as a Zeeman splitting with a strongly enhanced Landé factor. Within this approach, the exchange Hamiltonian $\hat{H}_{\rm ex}$ is given by

$$\hat{H}_{\rm ex} = -N_0\alpha x\frac{\hat{\sigma}_z}{2}\langle\hat{S}_z(B,T)\rangle_{\rm Mn}, \tag{6}$$

where N_0 is the number of unit cells per unit volume and $\langle\hat{S}_z\rangle_{\rm Mn}$ is the thermal average of the Mn^{2+} spin component along the z direction. The value $N_0\alpha = 0.22$ eV is commonly accepted for $Cd_{1-x}Mn_xTe$ for varying mole fraction x [24]. The thermal average $\langle\hat{S}_z\rangle_{\rm Mn}$ is calculated as a weighted sum over the components of the Zeeman-split ground multiplet,

$$\langle\hat{S}_z(B,T)\rangle_{\rm Mn^{2+}} = -S_0\mathfrak{B}_{5/2}\left(\frac{5}{2}\frac{g_{\rm Mn}\mu_B B}{k_B(T+T_0)}\right), \tag{7}$$

where $\mathfrak{B}_{5/2}(y)$ is the Brillouin function of order $5/2$. The phenomenological parameters S_0 (effective spin) and T_0 (effective temperature) account for the Mn-Mn interaction within the Mn-ion system. In $Cd_{1-x}Mn_xTe$ with $x = 0.016$ they assume the values $S_0 = 1.97$ and $T_0 = 1$ K [24,31–33].

By recollecting all Hamiltonian terms emerging from the approximate treatment of the magnetic impurities, we rewrite the initial Hamiltonian $\hat{H}$ as

$$\hat{H} = \frac{\mathbf{p}^2}{2m_e(z)} + \tilde{V}_\sigma(z), \tag{8}$$

with the spin-dependent potential

$$\tilde{V}_\sigma(z) = E_g + V(z) + \frac{\sigma}{2}[g_e\mu_B B_{\rm V} - N_0\alpha x\langle\hat{S}_z\rangle_{\rm Mn}\theta(z\in{\rm NQW})], \tag{9}$$

where $\theta(z\in{\rm NQW}) = 1$ inside the NQW and is equal to zero elsewhere. This Hamiltonian should be solved independently for $\sigma = \pm 1$.

Envelope function approach: Energy spectrum spin splitting and proximity effect

The envelope function method is based on expanding the wave function $\psi(\mathbf{r})$ as

$$\psi(\mathbf{r}) = f(\mathbf{r})u^{\Gamma_6}_{\mathbf{k}_0}(\mathbf{r}), \tag{10}$$

where $u^{\Gamma_6}_{\mathbf{k}_0}(\mathbf{r})$ is the Bloch function of the conduction band electrons (assumed to be the same in all layers of the heterostructure) and $f(\mathbf{r})$ is the so-called envelope function that changes slowly on the atomic scale. We neglect the anisotropy of the exchange interaction, as it is negligible in (Cd,Mn)Te, where the spin-orbit splitting at the Γ point is smaller than the energy gap. Furthermore, we assume the heterostructure is translationally invariant in the layer plane, which means that $f(\mathbf{r})$ can be factorized into a transversal plane wave and

a z-dependent function,

$$f(\mathbf{r}_\perp, z) = \frac{1}{\sqrt{\Phi}} \exp(i\mathbf{k}_\perp \mathbf{r}_\perp)\chi(z), \tag{11}$$

where the symbol $\perp$ indicates vectors oriented perpendicular to the heterostructure growth axis (Φ is the area of the sample cross section). The analog of the Hamiltonian (8) for the envelope function $\chi(z)$ in the simple case of a single parabolic band is called the Ben Daniel–Duke model. Its corresponding eigenproblem reads

$$\left[\tilde{V}_\sigma(z) - \frac{\hbar^2}{2}\frac{d}{dz}\frac{1}{m_e(z)}\frac{d}{dz} + \frac{\hbar^2 k_\perp^2}{2m_e(z)}\right]\chi_\sigma(z) = \varepsilon\chi_\sigma(z). \tag{12}$$

Here $m_e(z)$ is the effective electron mass of bulk materials. Similar to $\tilde{V}_\sigma(z)$, $m_e(z)$ is a piecewise-constant function of z with discontinuities at the interfaces. The effective mass $m_e = 0.12m_0$ in the spacer and barrier regions, while $m_e = 0.095m_0$ in the WQW and NQW. (The small fraction of manganese in CdTe has nearly no effect on the electron effective mass [30,34].) Note that, in order to calculate the exciton ground state while taking into account the contribution of the holes, we have renormalized the initial potential for the electrons by adjusting (increasing) the barrier width. This adjustment accounts for an additional electron confinement due to the adiabatic Coulomb potential created by the hole within the exciton.

The Ben Daniel–Duke eigenproblem is subject to additional continuity conditions; namely, $\chi_\sigma(z)$ and

$$\frac{1}{m_e(z)}\frac{d\chi_\sigma(z)}{dz}$$

must be continuous at each interface. Following a standard textbook procedure, we look for a solution within each layer in the form of either a free wave or an evanescent state. The continuity conditions will then be used to recast the eigenproblem into a system of transcendental equations for the adjustable parameters (the wave numbers) of our ansatz.

The system of linear equations has a nontrivial solution defined up to a normalization constant if the determinant of its matrix $\hat{M}_\sigma(\varepsilon)$ turns to zero. $\det\hat{M}_\sigma(\varepsilon) = 0$ is a complicated transcendental equation when solved with respect to the energy ε. Its solution gives the energy levels $\varepsilon_{\sigma,n}$ of the system and can be obtained only numerically.

To analyze the eigenstates of the conduction band electrons in our system of two coupled QWs under the influence of the external magnetic field, we first solve $\det\hat{M}_\sigma(\varepsilon) = 0$ for both spin projections σ and thus calculate the energy levels $\varepsilon_{\sigma,n}(B)$ in the practically relevant range $0 \leqslant B \leqslant 6$ T. When the magnetic field is applied to the heterostructure, the energy levels exhibit a nonlinear spin splitting. An additional contribution to the level splitting is present in the NQW, where the manganese ions are located. Figure 8 demonstrates the calculated ground exciton state in the WQW [Fig. 8(b)] and the state in the NQW [Fig. 8(a)], which directly reflect the Brillouin-like behavior as a function of magnetic field. The calculations were performed for a spacer width of 11 ML and a temperature $T = 1.6$ K. The red curves correspond to σ^+ polarization, and the black curves demonstrate σ^- polarization. As shown in Fig. 8, the presence of the Mn^{2+} ions in the NQW qualitatively modifies the simple linear Zeeman effect. In fact, the linear in B

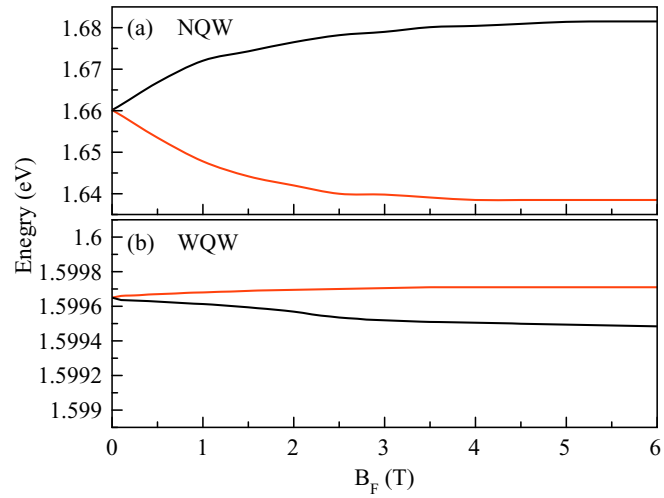

FIG. 8. Calculated state spectrum of a tunnel-coupled QW structure. Calculations were performed for the spacer width of 11 ML at temperature $T = 1.6$ K. Red curves correspond to σ^+ polarization, and black curves correspond to σ^- polarization.

splitting can still be seen at small fields, but it is massively overpowered by the exchange interaction contribution as the field gets stronger. The nonuniform growth of the splitting in the middle range of field strengths (up to 1–2 T) is the result of the subtle interplay between the exchange interaction and the spatial redistribution of the electron density. By looking at the splitting of the ground state [Fig. 8(b)], one finds that the energy dependence on the field strength for the spin-down electrons saturates at a certain value of magnetic field (about 2 T), while for the spin-up electrons the influence of the ions is negligible. The saturation effect is a result of the Mn^{2+} ion polarization. We attribute the difference between the measured [Fig. 2(d)] and the calculated [Fig. 8(b)] WQW exciton splittings to the calculation procedure. To simplify the calculations, we have included the effect of the holes in the model only on the phenomenological level by considering an additional electron confinement due to the adiabatic Coulomb potential created by the hole within the exciton. Indeed, in strong magnetic fields the localized ion momenta align with the field. Accordingly, the Brillouin function in Ref. [35], which describes the magnetization of the Mn^{2+} ions, reaches a plateau.

The present calculations were performed using the parameters of the material given above [effective masses $m^*(z)$, effective spin S_0, effective temperature T_0, exchange constant, and number of unit cells per unit αN_0, the mole fraction of manganese x] and the structural parameters of the double quantum well system (widths of the barrier, WQW and NQW, energy gaps for all materials). In the frame of our theoretical model we calculated the square of the overlap integral of the wave functions of the electron with the manganese ion $|\Psi_{e-Mn}|^2$, which directly determines the strength of the exchange interaction and differs for the resident electrons and the electrons bound in excitons.

We calculated the effective Landé factors as a function of temperature and spacer width for both the resident and exciton electrons. A comparison of the theoretical results with

experimentally measured data is shown in Figs. 4, 5, and 6. The experimentally obtained values of the g factors are well described by the proposed theoretical model. An exception is the value of the g factor for the second component at the lowest temperature.

V. CONCLUSIONS

The coherent spin dynamics of electrons has been studied in tunnel-coupled double quantum well structures [composed of a wide CdTe well and a narrow (Cd,Mn)Te well] with a narrow spacer between the wells using time-resolved pump-probe Kerr rotation. It has been shown that the spin dynamics of electrons in the wide QW is determined by the electron wave function penetration into the narrow QW and, consequently, by the strength of exchange interaction between the electrons and manganese ions in the narrow QW (short range proximity effect). The presence of two electron g factor components has been revealed, both of which depend on barrier thickness (proximity effect) and temperature. The observed difference in g factors is associated with two different subensembles of electrons and is caused by the stronger interaction of the resident electrons with manganese ions due to the weaker spatial localization of their wave function in comparison with the electrons bound in excitons. Despite the small penetration of the exciton wave function from the wide quantum well to the narrow one, the exciton interaction with the Mn^{2+} ions in the narrow quantum well was sufficient to launch their coherent spin precession.

ACKNOWLEDGMENTS

We are grateful to E. L. Ivchenko and M. M. Glazov for valuable advice and discussions. This work was financially supported by the Deutsche Forschungsgemeinschaft and the Russian Foundation for Basic Research through the International Collaborative Research Centre TRR 160 (Projects No. B4, A1, and Project No. 19-52-12066). V.N.M. acknowledges support from Grant No. 18-02-00052, and I.S.K. is grateful for the support from the U.S. DOE Office of Science via Grant No. DOE ER 46932. The research in Poland was partially supported by the National Science Centre (NCN) of Poland through Grants No. 2017/25/B/ST3/02966 and No. 2018/30/M/ST3/00276.

[1] *Optical Orientation*, edited by F. Meier and B. P. Zakharchenya (North-Holland, New York, 1984).

[2] *Introduction to the Physics of Diluted Magnetic Semiconductors*, edited by J. Kossut and J. A. Gaj (Springer, Berlin, 2010).

[3] *Semiconductor Spintronics and Quantum Computation*, edited by D. D. Awschalom, D. Loss, and N. Samarth (Springer, Berlin, 2002).

[4] S. Cronenberger, M. Vladimirova, S. V. Andreev, M. B. Lifshits, and D. Scalbert, Optical Pump-Probe Detection of Manganese Hyperfine Beats in (Cd, Mn)Te Crystals, Phys. Rev. Lett. **110**, 077403 (2013).

[5] K. A. Baryshnikov, L. Langer, I. A. Akimov, V. L. Korenev, Yu. G. Kusrayev, N. S. Averkiev, D. R. Yakovlev, and M. Bayer, Resonant optical alignment and orientation of Mn^{2+} spins in CdMnTe crystals, Phys. Rev. B **92**, 205202 (2015).

[6] P. Faltermeier, G. V. Budkin, J. Unverzagt, S. Hubmann, A. Pfaller, V. V. Bel'kov, L. E. Golub, E. L. Ivchenko, Z. Adamus, G. Karczewski, T. Wojtowicz, V. V. Popov, D. V. Fateev, D. A. Kozlov, D. Weiss, and S. D. Ganichev, Magnetic quantum ratchet effect in (Cd, Mn)Te- and CdTe-based quantum well structures with a lateral asymmetric superlattice, Phys. Rev. B **95**, 155442 (2017).

[7] E. A. Zhukov, Yu. G. Kusrayev, K. V. Kavokin, D. R. Yakovlev, J. Debus, A. Schwan, I. A. Akimov, G. Karczewski, T. Wojtowicz, J. Kossut, and M. Bayer, Optical orientation of hole magnetic polarons in (Cd, Mn)Te/(Cd, Mn, Mg)Te quantum wells, Phys. Rev. B **93**, 245305 (2016).

[8] Z. Ben Cheikh, S. Cronenberger, M. Vladimirova, D. Scalbert, F. Perez, and T. Wojtowicz, Electron spin dephasing in Mn-based II-VI diluted magnetic semiconductors, Phys. Rev. B **88**, 201306(R) (2013).

[9] C. Rice, L. C. Smith, J. J. Davies, D. Wolverson, M. Wiater, G. Karczewski, and T. Wojtowicz, Exchange interactions in $Cd_{1-x}Mn_xTe$ wide quantum wells, Phys. Rev. B **86**, 155318 (2012).

[10] I. A. Merkulov, D. R. Yakovlev, A. Keller, W. Ossau, J. Geurts, A. Waag, G. Landwehr, G. Karczewski, T. Wojtowicz, and J. Kossut, Kinetic Exchange between the Conduction Band Electrons and Magnetic Ions in Quantum-Confined Structures, Phys. Rev. Lett. **83**, 1431 (1999).

[11] T. Koga, J. Nitta, H. Takayanagi, and S. Datta, Spin-Filter Device Based on the Rashba Effect Using a Nonmagnetic Resonant Tunneling Diode, Phys. Rev. Lett. **88**, 126601 (2002).

[12] A. Voskoboynikov, S. S. Liu, and C. P. Lee, Spin-dependent electronic tunneling at zero magnetic field, Phys. Rev. B **58**, 15397 (1998).

[13] N. S. Maslova, P. I. Arseyev, and V. N. Mantsevich, Control of the non-stationary spin-polarized tunneling currents by applied bias changing, Solid State Comm. **248**, 21 (2016).

[14] V. N. Mantsevich, I. V. Rozhansky, N. S. Maslova, P. I. Arseyev, N. S. Averkiev, and E. Lähderanta, Mechanism of ultrafast spin-polarization switching in nanostructures, Phys. Rev. B **99**, 115307 (2019).

[15] D. R. Yakovlev and W. Ossau, Magnetic polarons, in *Introduction to the Physics of Diluted Magnetic Semiconductors*, edited by J. Kossut and J. A. Gaj (Springer, Berlin, 2010), Chap. 7, pp. 221–263.

[16] W. D. Rice, W. Liu, V. Pinchetti, D. R. Yakovlev, V. I. Klimov, and S. A. Crooker, Direct measurements of magnetic polarons in $Cd_{1-x}Mn_xSe$ nanocrystals from resonant photoluminescence, Nano Lett. **17**, 3068 (2017).

[17] I. A. Akimov, V. L. Korenev, V. F. Sapega, L. Langer, S. V. Zaitsev, Yu. A. Danilov, D. R. Yakovlev, and M. Bayer, Orientation of electron spins in hybrid ferromagnet-semiconductor nanostructures, Phys. Status Solidi B **251**, 1663 (2014).

[18] V. L. Korenev, M. Salewski, I. A. Akimov, V. F. Sapega, L. Langer, I. V. Kalitukha, J. Debus, R. I. Dzhioev, D. R. Yakovlev, D. Müller, C. Schröder, H. Hövel, G. Karczewski, M. Wiater, T. Wojtowicz, Yu. G. Kusrayev, and M. Bayer,

Long-range $p-d$ exchange interaction in a ferromagnet-semiconductor hybrid structure, Nat. Phys. **12**, 85 (2016).

[19] V. L. Korenev, I. V. Kalitukha, I. A. Akimov, V. F. Sapega, E. A. Zhukov, E. Kirstein, O. S. Ken, D. Kudlacik, G. Karczewski, M. Wiater, T. Wojtowicz, N. D. Ilyinskaya, N. M. Lebedeva, T. A. Komissarova, Yu. G. Kusrayev, and M. Bayer, Low voltage control of exchange coupling in a ferromagnet-semiconductor quantum well hybrid structure, Nat. Commun. **10**, 2899 (2019).

[20] I. Žutić, J. Fabian, and S. C. Erwin, Spin Injection and Detection in Silicon, Phys. Rev. Lett. **97**, 026602 (2006).

[21] J. M. Kikkawa and D. D. Awschalom, Resonant Spin Amplification in *n*-Type GaAs, Phys. Rev. Lett. **80**, 4313 (1998).

[22] A. A. Sirenko, T. Ruf, M. Cardona, D. R. Yakovlev, W. Ossau, A. Waag, and G. Landwehr, Electron and hole g factors measured by spin-flip Raman scattering in CdTe/$Cd_{1-x}Mg_x$Te single quantum wells, Phys. Rev. B **56**, 2114 (1997).

[23] G. Bartsch, M. Gerbracht, D. R. Yakovlev, J. H. Blokland, P. C. M. Christianen, E. A. Zhukov, A. B. Dzyubenko, G. Karczewski, T. Wojtowicz, J. Kossut, J. C. Maan, and M. Bayer, Positively versus negatively charged excitons: A high magnetic field study of CdTe/$Cd_{1-x}Mg_x$Te quantum wells, Phys. Rev. B **83**, 235317 (2011).

[24] J. Gaj, Semimagnetic semiconductors, Acta Phys. Pol. A **96**, 651 (1999).

[25] E. A. Zhukov, D. R. Yakovlev, M. Gerbracht, G. V. Mikhailov, G. Karczewski, T. Wojtowicz, J. Kossut, and M. Bayer, Spin coherence of holes and electrons in undoped CdTe/(Cd, Mg)Te quantum wells, Phys. Rev. B **79**, 155318 (2009).

[26] E. A. Zhukov, D. R. Yakovlev, M. Bayer, M. M. Glazov, E. L. Ivchenko, G. Karczewski, T. Wojtowicz, and J. Kossut, Spin coherence of a two-dimensional electron gas induced by resonant excitation of trions and excitons in CdTe/(Cd, Mg)Te quantum wells, Phys. Rev. B **76**, 205310 (2007).

[27] G. Bastard, *Wave Mechanics Applied to Semiconductor Heterostructures*, Monographies de physique (Les Ulis Cedex, France, 1988).

[28] A. V. Kavokin, V. P. Kochereshko, G. R. Posina, I. N. Uraltsev, D. R. Yakovlev, G. Landwehr, R. N. Bicknell-Tassius, and A. Waag, Effect of the electron Coulomb potential on hole confinement in II-VI quantum wells, Phys. Rev. B **46**, 9788 (1992).

[29] E. G. LeBlanc, M. Edirisooriya, O. S. Ogedengbe, O. C. Noriega, P. A. R. D. Jayathilaka, S. Rab, C. H. Swartz, D. R. Diercks, G. L. Burton, B. P. Gorman, A. Wang, T. M. Barnes, and T. H. Myers, Determining and controlling the magnesium composition in CdTe/CdMgTe heterostructures, J. Electron. Mater. **46**, 5379 (2017).

[30] *Semiconductors: II-VI and I-VII Compounds; Semimagnetic Compounds*, Landolt-Börnstein, New series, Group 3 Condensed Matter, Vol. III/41-B, edited by O. Madelung, U. Rössler, and M. Schulz (Springer, Berlin, 1999).

[31] C. Lewiner, J. A. Gaj, and G. Bastard, Indirect exchange interaction in $Hg_{1-x}Mn_x$Te and $Cd_{1-x}Mn_x$Te alloys, J. Phys. Colloques **41**, C5-289 (1980).

[32] W. J. Ossau and B. Kuhn-Heinrich, Dimensional dependence of antiferromagnetism in diluted magnetic semiconductor heterostructures, Phys. B (Amsterdam, Neth.) **184**, 422 (1993).

[33] D. R. Yakovlev, G. Mackh, B. Kuhn-Heinrich, W. Ossau, A. Waag, G. Landwehr, R. Hellmann, and E. O. Göbel, Exciton magnetic polarons in short-period CdTe/(Cd, Mn)Te superlattices, Phys. Rev. B **52**, 12033 (1995).

[34] M. Inoue, Electrical properties of n-type $Cd_{1-x}Mg_x$Te, J. Phys. Soc. J. **26**, 1186 (1969).

[35] J. A. Gaj, J. Ginter, and R. R. Galazka, Exchange interaction of manganese $3d^5$ states with band electrons in $Cd_{1-x}Mn_x$Te, Phys. Status Solidi B **89**, 655 (1978).